Argon Cluster-Mediated Trapping and Vibrational Spectroscopic Characterization of an $OH^-\cdot HCH_2^\bullet$ Intermediate in the $O^{\bullet-} + CH_4$ Reaction

Eric G. Diken, Gary H. Weddle,‡ Jeffrey M. Headrick, J. Mathias Weber,† and Mark A. Johnson*

Sterling Chemistry Laboratory, Yale University, P.O. Box 208107, New Haven, Connecticut 06520-8107

Received: June 21, 2004

We isolate an $[O\cdot CH_4]^{\bullet-}$ intermediate in the reactive $O^{\bullet-} + CH_4$ encounter using an argon cluster-mediated trapping technique and characterize it using vibrational predissociation spectroscopy. The spectra of the argon-solvated complexes establish that only the $OH^-\cdot CH_3^\bullet$ ion−radical adduct is prepared. Its formation is firmly established by the appearance of the signature OH^- stretching band close to that of the free hydroxide ion. The band origin locations and partially resolved rotational spacings indicate that hydroxide binds onto one of the methyl hydrogen atoms, much like the motif observed previously in the $I^-\cdot HCH_2^\bullet$ ion−radical complex. This $OH^-\cdot CH_3^\bullet$ species is best regarded as an entrance-channel complex in the secondary (endothermic) $OH^- + CH_3^\bullet \rightarrow H_2O + CH_2^-$ proton transfer reaction. These observations indicate that the initial H-atom abstraction step ($O^{\bullet-} + CH_4 \rightarrow OH^- + CH_3^\bullet$) occurs too quickly to enable capture of the intermediates directly associated with this process.

I. Introduction

The chemistry of the $O^{\bullet-}$ radical anion (^2P) with alkanes and alkenes (RH_2) has been extensively studied over the past 30 years,[1−9] largely because it presents several unique features nicely summarized in the review article by Lee and Grabowski.[10] Its pattern of reactivity derives from the fact that the proton transfer channel (leading to $OH^\bullet + RH^{\bullet-}$) is endothermic, while H-atom abstraction

$$O^{\bullet-} + RH_2 \rightarrow OH^- + RH^\bullet \quad (1)$$

occurs with a low barrier and is typically exothermic. Interestingly, when the very basic hydroxide ion product of reaction 1 remains in the vicinity of the nascent hydrocarbon radical, the proton transfer process then becomes operative in a second step

$$OH^- + RH^\bullet \rightarrow H_2O + R^- \quad (2)$$

leading to the production of carbene anions.[5,10] This propensity was, in fact, exploited[11,12] to great effect as a preparative route to the vinylidene anion, $CH_2{=}C^-$, by the reaction of $O^{\bullet-}$ with ethylene.

In this paper, we focus on the simplest of these reactions[7]

$$O^{\bullet-} + CH_4 \rightarrow OH^- + CH_3^\bullet + 0.26\ \text{eV} \quad (3)$$

where, in the case of methane, the second, proton transfer step (leading to $H_2O + CH_2^-$) is endothermic and, therefore, is not available at the low collision energies explored in this work. Viggiano and co-workers[3,5] have recently reported the kinetics of reaction 3 and discussed their results in the context of the potential surface illustrated in Figure 1. This is a standard double-minimum construction[13] that supports two local minima. These correspond to the entrance- and exit-channel complexes of reaction 3, which are separated by the transition-state barrier. Like the case of the classic S_N2 reaction (e.g., $Cl^- + CH_3Br$), the barrier is calculated to lie below the asymptotic energy of the reactants,[3] presenting the possibility of trapping reaction intermediates in these minima and characterizing them using photoelectron and vibrational spectroscopies.[14,15] Here, we exploit the argon-mediated synthetic methodology developed at Yale[16,17] to capture $[O\cdot CH_4]^{\bullet-}$ intermediates in reaction 3

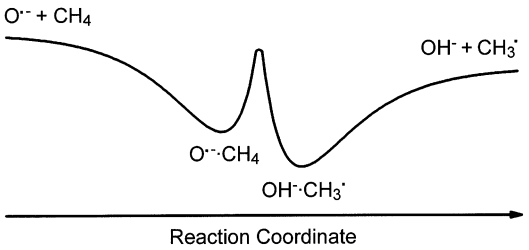

Figure 1. Potential energy curve (schematic drawing) depicting the reaction coordinate ($O^{\bullet-}\cdots H\cdots CH_3$) for the $O^{\bullet-} + CH_4 \rightarrow OH^- + CH_3^\bullet$ hydrogen atom abstraction reaction. The minima correspond to the $O^{\bullet-}\cdot CH_4$ and $OH^-\cdot CH_3^\bullet$ entrance- and exit-channel reaction intermediates, respectively.

$$O^{\bullet-}\cdot Ar_n + CH_4 \rightarrow [O\cdot CH_4]^{\bullet-}\cdot Ar_m + (n-m)Ar. \quad (4)$$

This approach has significant advantages in that the intermediates are vibrationally cooled by the evaporation of weakly bound argon atoms, and when argon atoms are retained upon condensation of methane, the trapped species can be characterized using argon predissociation vibrational spectroscopy[18]

$$[O\cdot CH_4]^{\bullet-}\cdot Ar_m + h\nu \rightarrow [O\cdot CH_4]^{\bullet-} + m\text{Ar}. \quad (5)$$

One expects that the structures of the entrance- and exit-channel intermediates ($O^{\bullet-}\cdot CH_4$ and $OH^-\cdot CH_3^\bullet$, respectively)

* To whom correspondence should be addressed. E-mail: mark.johnson@yale.edu.

† Present address: Institut für Physikalische Chemie, Universität Karlsruhe, Kaiserstr. 12, D-76128 Karlsruhe, Germany.

‡ Present address: Fairfield University Department of Chemistry, Fairfield, CT 06430.

10.1021/jp0404403 CCC: $27.50
Published on Web 10/19/2004

can be readily distinguished by their differing mid-infrared spectra. Specifically, the $O^{\bullet-}\cdot CH_4$ ion−molecule complex should, in an analogy with the halide−methane complexes studied extensively by Bieske and co-workers,[19,20] yield a characteristic pattern of bands in the C−H stretching region associated with the methyl group (2500−3000 cm^{-1}), while the $OH^-\cdot CH_3^\bullet$ exit-channel species can be expected to display a band at much higher energy arising from the OH^- moiety. We will show that the argon evaporation method yields only the species derived from the exit channel, suggesting that either the barrier to reaction is small or the lifetime of the collision complex in the entrance channel is short as compared to the time scale for argon evaporation.

II. Experimental Section

The $[O\cdot CH_4]^{\bullet-}\cdot Ar_m$ clusters were generated by the entrainment of trace CH_4 and N_2O vapors through independently controlled pulsed valves into a supersonic expansion of pure argon (∼4-atm backing pressure).[17] The pulsed expansion (10 Hz) was ionized by a counter-propagating 1 keV electron beam, primarily yielding clusters of the type $O^{\bullet-}\cdot Ar_n$ ($n < 20$) by dissociative electron attachment onto $N_2O\cdot Ar_n$ clusters.[21,22] The CH_4 molecules were then condensed onto the argon-solvated $O^{\bullet-}$ clusters so that the collision complexes could be stabilized into local minima of the reactive potential energy surface by the rapid evaporation of argon atoms. The $[O\cdot CH_4]^{\bullet-}\cdot Ar_m$ cluster ions were injected into the Yale tandem time-of-flight photofragmentation spectrometer described previously.[23] Mid-infrared spectra of the $[O\cdot CH_4]^{\bullet-}\cdot Ar_m$ species were obtained using argon predissociation spectroscopy [eq 5],[18] where the tunable mid-IR radiation was generated using a 10 Hz Nd:YAG pumped, KTP/KTA-based optical parametric oscillator (LaserVision). This source delivers approximately 5 mJ/pulse in the 3000 cm^{-1} range in a bandwidth of about 3 cm^{-1}. The reported spectra are normalized for variations in the laser output energy over the entire scan range and result from an accumulation of 15−40 individual scans. The absolute wavenumber calibration of this instrument is ±5 cm^{-1}.

III. Computational Details

Preliminary calculations (*Gaussian 98*[24] and *TURBOMOLE*[25]) were performed at both the B3LYP and MP2 levels of theory, with various basis sets as indicated to explore the possible structures and harmonic vibrational frequencies of the $[O\cdot CH_4]^{\bullet-}$ and $OH^-\cdot CH_4$ complexes. We also examined the potential surface for intracluster proton transfer by optimizing the molecular geometries for fixed values of the (scanned) C−H stretching coordinates (Figure 6). This was carried out using the triple-ζ valence basis sets including diffuse polarizable functions (TZVP and TZVPP).[26] In the DFT calculations, the exchange correlation energy was calculated using a grid of medium density (m3).

IV. Results and Discussion

IV. A. Spectral Signature of an Embedded Hydroxide Anion. The vibrational predissociation spectrum of the $[O\cdot CH_4]^{\bullet-}\cdot Ar_4$ cluster (detected via the loss of four argon atoms) is presented in Figure 2a. Most importantly, there is a sharp band at 3586 cm^{-1}, close to the origin for the isolated hydroxide stretch (arrow in Figure 2a) measured by Saykally and co-workers using velocity-modulated absorption spectroscopy.[27] This immediately signals the presence of a more or less intact hydroxide moiety and suggests that we have trapped the $OH^-\cdot CH_3^\bullet$ exit-channel complex in reaction 3.

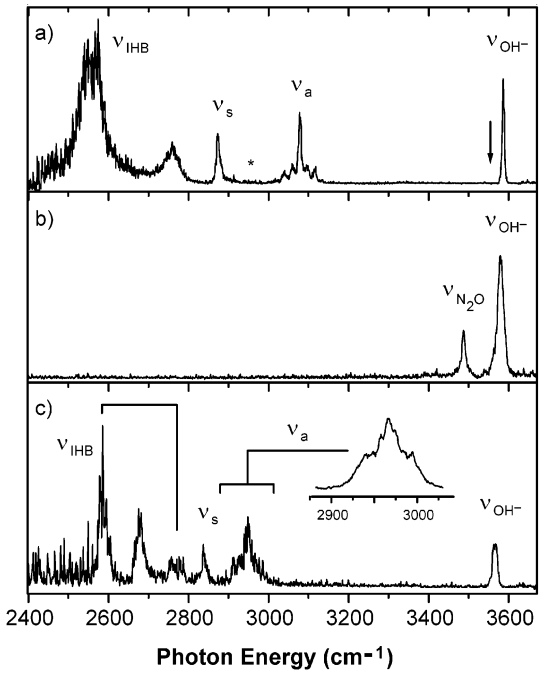

Figure 2. Mid-infrared spectra for the (a) $OH^-\cdot CH_3^\bullet\cdot Ar_4$, (b) $OH^-\cdot N_2O$, and (c) $OH^-\cdot CH_4\cdot Ar_1$ complexes. The hydrocarbon species a and c were detected by argon predissociation, whereas the $OH^-\cdot N_2O$ binary complex was detected via loss of the weakly bound N_2O molecule. In the C−H stretching region ($h\nu < 3200$ cm^{-1}), the labels ν_{IHB}, ν_s, and ν_a correspond to the fundamental vibrations for the ionic H-bonded C−H stretch and the nonbonded symmetric and asymmetric $-CH_2$ ($-CH_3$) stretches, respectively. The asterisk (*) in the upper trace indicates the predicted position for the asymmetric C−H stretching band origin for the $O^{\bullet-}\cdot CH_4$ entrance-channel complex. In the region above 3200 cm^{-1}, ν_{OH^-} denotes the hydroxide stretch, while ν_{N_2O} refers to the $\nu_1 + \nu_3$ combination band involving the N−N and N−O stretches in isolated N_2O. The arrow in the upper trace indicates the position of the OH stretch in isolated OH^- (ref 27).

To explore the position and character of the hydroxide stretching transition in an ion−molecule (as opposed to an ion−radical) complex, we include in Figure 2b the spectrum of the nonreactive $OH^-\cdot N_2O$ cluster (detected via the loss of N_2O). This species displays a band (3579 cm^{-1}) only 7 cm^{-1} below that found in $OH^-\cdot CH_3^\bullet$, along with a second, less intense feature at 3487 cm^{-1}. The latter transition (denoted υ_{N_2O} in Figure 2b) appears 21 cm^{-1} lower in energy than the $\nu_1 + \nu_3$ band origin in isolated N_2O (3508 cm^{-1}),[28] confirming that the N_2O component is indeed essentially neutral. Consequently, the associated OH^- constituent can be regarded as a predominantly charge-localized hydroxide anion in the binary complex.

As a second example more relevant to the hydrocarbon case of primary interest, we also obtained the spectrum of the $OH^-\cdot CH_4\cdot Ar$ complex (detected via loss of the argon atom), with the result shown in Figure 2c. Once again, a single isolated feature appears at high energy (3566 cm^{-1}) and is readily assigned to the OH^- ion, while much more structure is evident toward lower energy as will be discussed further. The important conclusion drawn from these related systems is that, when present, the hydroxide ion yields a simple, isolated spectral signature even when strongly bound as either an ion−molecule or ion−radical complex.

IV. B. Rotational Fine Structure in the C−H Stretching Bands. The occurrence of the characteristic OH^- stretching band in the $[O\cdot CH_4]^{\bullet-}$ ion ensemble conclusively establishes the formation of the $OH^-\cdot CH_3^\bullet$ ion−radical complex. However, to examine the structure of this (nominally) exit-channel species

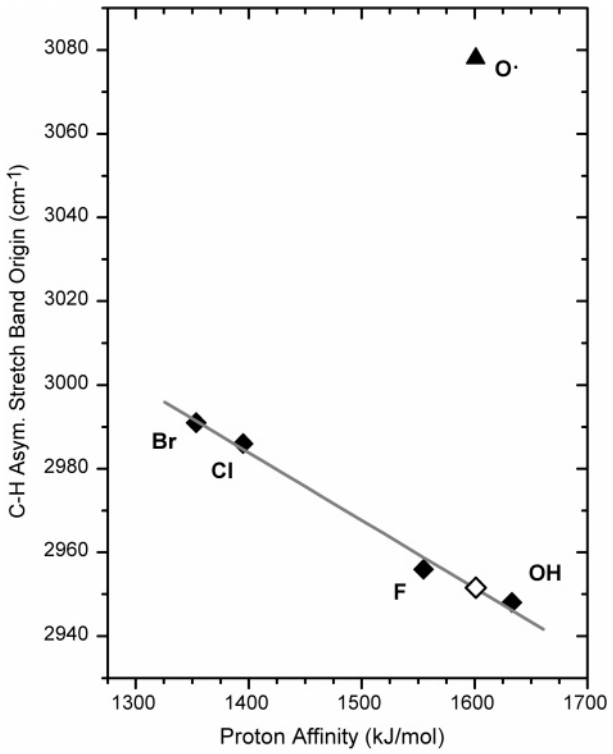

Figure 3. Band origins (cm^{-1}) for the nonbonded, asymmetric $-CH_3$ stretching vibration for various complexes $X^-\cdot CH_4$ (X = Br, Cl, F, O•, and OH), plotted as a function of the ion's proton affinity (kJ/mol). The open diamond (◇) designates the extrapolated asymmetric stretching band origin predicted for the $O^{\bullet-}\cdot CH_4$ entrance-channel (methane intact) based on this trend. The origin of the observed $-CH_3$ perpendicular band from the $[O\cdot CH_4]^{\bullet-}$ complex (▲) lies far above this expected value. The values for the halide−methane binary complexes are taken from refs 19 and 20.

as well as the possibility that the $O^{\bullet-}\cdot CH_4$ entrance-channel complex is also prepared, we turn our attention to the C−H stretching region. In previous studies of the $X^-\cdot CH_4$ (X = F, Cl, and Br) ion−molecule complexes reported by Bieske and co-workers,[19,20] the halide ions hydrogen bond to only one of the hydrogen atoms (as opposed to the methyl pocket[29] or bifurcated motifs), resulting in C_{3v} symmetry adducts. This arrangement breaks the degeneracy of the vibrations in the highly symmetric CH_4 molecule and activates the nominally IR forbidden symmetric stretching vibration. The C−H stretch normal modes thus evolve into a unique, partially decoupled stretch for the hydrogen bound to the ion, with the remaining three vibrations arising largely from the motion of the three nonbonded hydrogen atoms. These modes occur as nondegenerate (ν_s) symmetric and degenerate (ν_a) asymmetric stretching vibrations. In the $O^{\bullet-}$ case, we introduce the further complication that, should an $O^{\bullet-}\cdot CH_4$ isomer be present, there may be low-lying electronic states arising from the splitting of the degeneracies inherent to the open-shell (^2P) nature of this species.

In the C_{3v} complexes, the degenerate ν_a band is the highest in energy of the C−H stretching fundamentals, and this transition has been reported[19,20,30] to systematically red-shift with increasing proton affinity of the halide ion in the $X^-\cdot CH_4$ complexes, as illustrated in Figure 3. Our spectrum of $OH^-\cdot CH_4$ (Figure 2c) thus allows us to further explore this propensity beyond the halide anions. In addition to its location, the asymmetric stretch assignment [labeled (ν_a)] is supported by the broadened, but symmetrical rotational envelope (see enhanced signal-to-noise inset scan in Figure 2c). In the $X^-\cdot CH_4$ halide complexes, this perpendicular band appears with the well-resolved K-stack structure arising from rotation of the hydrogen atoms about the symmetry axis. With this assignment, we conclude that the hydroxide ion yields the largest red-shift observed to date, but does so in keeping with the overall trend set by the halides (see Figure 3).

The remaining, very red-shifted C−H stretching bands in the $OH^-\cdot CH_4$ spectrum can be assigned to the parallel symmetric stretching vibration (ν_s) associated with the three free hydrogen atoms and to excitation of the hydrogen atom bound to the OH^- ion (labeled ν_{IHB} to indicate the ionic H-bond in Figure 2c). Note that the IHB vibration is accompanied by two other bands just above it, as is typical with the complexity introduced by excitation of the shared proton in strongly H-bonded systems [e.g., $X^-\cdot HOR$].[31] In this case, the band appearing ~180 cm^{-1} above the IHB fundamental matches the calculated energy (B3LYP/TZVP level) of the ion−molecule stretching mode, while assignment of the other band closer to the IHB origin is ambiguous. Likely candidates include the C−H bending overtone and another soft-mode excitation in combination with the IHB fundamental, possibly involving the out-of-plane wag.

With the behavior of the $OH^-\cdot CH_4$ complex in mind, we can address the possibility that the entrance-channel complex, $O^{\bullet-}\cdot CH_4$, contributes to the observed spectrum in Figure 2a. Note that, like the $OH^-\cdot CH_4$ spectrum, the highest-energy $[O\cdot CH_4]^{\bullet-}\cdot Ar_4$ band in the C−H stretching region (band origin ~3078 cm^{-1}) appears with a resolved rotational envelope signaling a perpendicular transition (labeled ν_a). The next feature toward lower energy (2873 cm^{-1}) is sharp, as expected for a parallel band (labeled ν_s). Recall that the neutral methyl radical C−H stretches fall about 100 cm^{-1} higher in energy than those in isolated CH_4.[28]

To search for features attributable to $O^{\bullet-}\cdot CH_4$, we can estimate where the asymmetric stretch would occur for a putative $O^{\bullet-}\cdot CH_4$ C_{3v} structure using the proton affinity trend displayed in Figure 3. The extrapolated value for $O^{\bullet-}\cdot CH_4$ is included as an open diamond (◇) in Figure 3 and is also marked on the spectrum in Figure 2a by an asterisk (*). Because no absorption is recovered near this expected value and the nearby transitions are expected for the $OH^-\cdot CH_3^\bullet$ complex, we conclude that the entrance-channel intermediate is not, in fact, isolated in the present experimental arrangement.

The fine structure associated with the ν_a band in the $OH^-\cdot CH_3^\bullet$ complex (Figure 2a) provides crucial clues for the elucidation of its structure. It is especially useful to compare its spectrum with that obtained previously[21] for the $I^-\cdot HCH_2^\bullet$ complex, and the two spectra are displayed in Figure 4. In the $I^-\cdot HCH_2^\bullet$ case, this planar C_{2v} complex occurs with the ion bound to one of the hydrogen atoms (see the structure above the top trace in Figure 4). This geometry yields three IR-active C−H stretching fundamentals, two parallel transitions, and one perpendicular transition, with the latter lying highest in energy. The dominant feature in the $I^-\cdot HCH_2^\bullet$ spectrum (upper trace in Figure 4) occurs lowest in energy and arises from excitation of the hydrogen bound to the ion, while the free hydrogen atoms contribute the two almost-overlapping transitions at higher energy. The sharper parallel band arising from the symmetric $-CH_2$ stretch is embedded in the more open rotational envelope corresponding to the perpendicular asymmetric $-CH_2$ stretch, with a splitting of only 13 cm^{-1} between the band origins.

Turning to the $OH^-\cdot CH_3^\bullet$ spectrum in the C−H stretching region (lower trace in Figure 4), the higher energy, perpendicular band displays a remarkably similar rotational profile to that found in $I^-\cdot HCH_2^\bullet$, strongly suggesting that they share a common structural motif. In fact, the pattern is simpler in the

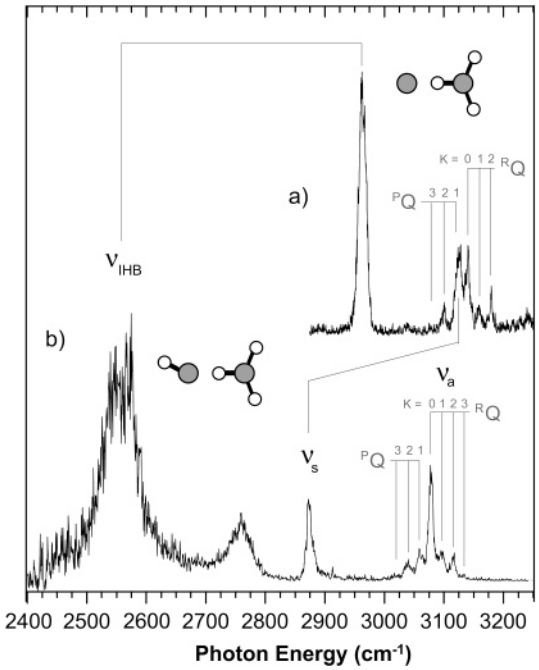

Figure 4. Mid-infrared spectra of the (a) $I^-\cdot CH_3^\bullet\cdot Ar$ and (b) $OH^-\cdot CH_3^\bullet\cdot Ar_4$ hydrogen-bonded ion−radical complexes. The labeled brackets (grey) indicate the rotational Q-branch assignments in the perpendicular asymmetric stretching vibration. See Figure 2 caption for definitions of band labels.

$OH^-\cdot CH_3^\bullet$ spectrum, because the sharper parallel band, which is also present but blended with the $^PQ(1)$ band in the $I^-\cdot HCH_2^\bullet$ spectrum, now appears about 205 cm^{-1} below it. In this scenario, the dominant bands in the $OH^-\cdot HCH_2^\bullet$ spectrum, which can be traced to excitation of the hydrogen bound to the ion, are the most red-shifted (relative to the bands of the isolated $CH_3^\bullet$ radical) and appear with the most broadening. The proposed structure is sketched above the lower trace in Figure 4.

To further analyze the structural information in the rotational profiles, Figure 5 presents an expanded comparison of the ν_a bands observed for the $I^-\cdot HCH_2^\bullet$ and $OH^-\cdot HCH_2^\bullet$ complexes, where they are shifted to a common origin. In the C_{2v} symmetry $I^-\cdot HCH_2^\bullet$ complex, the Q-branches arising from the K-stacks are spaced by $2B \approx 20$ cm^{-1} and appear somewhat staggered in their intensity profile. The latter is expected from nuclear spin statistics, which result in a 3:1 alternating intensity profile favoring even K. Note that the peak spacing and intensity behavior unambiguously identify the carrier as C_{2v} as opposed to a C_{3v} symmetry species, where the latter should display a 2:1:1:2 intensity alternation with K, as well as a more compact (by a factor of 2) Q-branch spacing. The more open rotational spacing in $OH^-\cdot HCH_2^\bullet$ is almost exactly the same as that found in the $I^-\cdot HCH_2^\bullet$ complex (19.9 vs 19.6 cm^{-1} for the iodide and hydroxide complexes, respectively). We therefore, conclude that, in the $OH^-\cdot CH_3^\bullet$ complex, only two nonbonded hydrogen atoms contribute to the $\Delta K = \pm 1$ rotational envelopes associated with the perpendicular transition. We will next consider the structural implications of this observation.

IV. C. Comments on Internal Rotation and Band Profiles in the Context of Theoretical Structures. The characterization of the observed $OH^-\cdot CH_3^\bullet$ species as a single H-bonded, pseudo-C_{2v} ($OH^-\cdot HCH_2^\bullet$) species is strongly supported by the empirical analysis of the spectra. This behavior is surprising, because, although this single H-bonded motif is indeed calculated to be a local minimum structure at all explored levels of theory, the hydrogen atom associated with the OH^- moiety

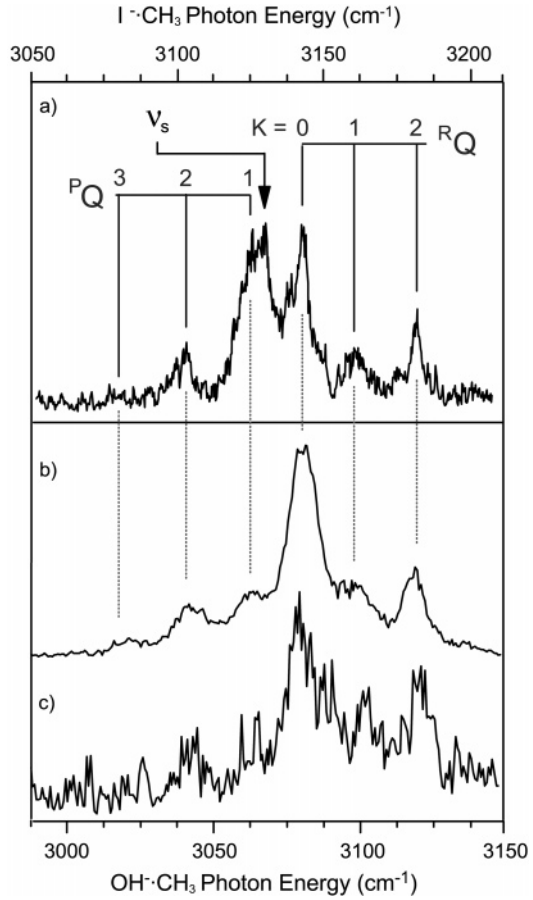

Figure 5. Comparison of the C−H asymmetric stretching (ν_a) bands, shifted to a common origin, for the (a) $I^-\cdot CH_3^\bullet\cdot Ar$ and the $OH^-\cdot CH_3^\bullet\cdot Ar_n$ ion−radical complexes with (b) $n = 4$ and (c) $n = 5$. The low-resolution (~3 cm^{-1} bandwidth) argon predissociation spectra display partially resolved rotational structure and nuclear spin statistics consistent with C_{2v} symmetry complexes.

always lies away from the $O-CH_2$ symmetry axis in the equilibrium geometry. That is, the C_{2v} structure, with the hydroxide H-atom lying on the symmetry axis, is calculated to be a transition state. Two aspects of this are perplexing: First, the off-axis OH^- stretch would be expected to support a perpendicular transition, as observed previously for the free OH stretch transition in the $I^-\cdot HDO$ complex.[32] The OH^- stretch in $OH^-\cdot HCH_2^\bullet$ (and the other complexes studied here) is, however, always observed to be sharp, as would be expected for a parallel transition. Second, one might expect that the off-axis H-atom of the OH^- species would contribute to the moment of inertia for rotation of the complex about the O···C axis, while the observed ν_a pattern is almost identical to that found for $I^-\cdot HCH_2^\bullet$. One clue to this apparent paradox is the observation that the location of the hydroxide hydrogen varies dramatically with the level of theory and basis sets used. Not surprisingly, these structures occur with very small force constants for internal rotation of the oxygen-bound hydrogen atom. Thus, an important feature of this complex that warrants further theoretical work is to define the potential surface governing the (frustrated) internal rotation of the hydroxide motion. A very low barrier, for example, might yield large amplitude zero-point motion that would result in a (zero-point) vibrationally averaged structure that preserves C_{2v} symmetry.

As a final comment on the observed rotational patterns, we note that the spectrum shown in Figure 2a was obtained with four argon atoms, indicating that the $-CH_2$ rotation occurs as an internal motion within the argon-solvated complex. To

explore whether this can be suppressed with the further addition of argon atoms, we also obtained the spectrum of the $OH^-\cdot HCH_2^\bullet\cdot Ar_5$ complex with the result shown in Figure 5c. While this spectrum clearly suffers from a lower signal-to-noise ratio, the outline of the rotational envelope is clear and displays the same spacing as that found in the smaller cluster. Thus, the internal rotational motion appears to be very robust with respect to perturbation by weakly bound argon atoms. The phenomenon was also encountered in the $I^-\cdot HCH_2^\bullet$ case.[21] Interestingly, this persistence of internal rotation was not observed in the C_{3v} pocket-bound intermediates in the S_N2 reaction, $Cl^-\cdot CH_3Br$.[29]

IV. D. Remarks on the Sequential Reaction Pathway and Nature of the Potential Surface. The analysis of the rotation−vibration spectrum establishes that the $OH^-\cdot CH_3^\bullet$ complex consists of a hydroxide ion bound to one of the hydrogen atoms in the methyl radical. This structure is interesting in light of the general discussion presented in the Introduction regarding the characteristic two stages of $O^{\bullet-} + RH_2$ chemistry, in which the first step involves H-atom abstraction (eq 1) and the second step corresponds to proton transfer (eq 2). It is clear that the intermediate leading to the first step, $O^{\bullet-}\cdot CH_4$, could not be isolated using argon-mediated trapping, suggesting that H-atom abstraction is too fast to be quenched into a local minimum prior to reaction. The second, exit-channel minimum sketched in Figure 1 would correspond to the $OH^-\cdot CH_3^\bullet$ (carbon-bound) complex with an O−H−CH_3 bonding motif. This is also not the complex isolated in our experiment. Instead, after hydrogen atom abstraction, the nascent OH^- ion migrates to a second hydrogen atom and, in effect, begins the second, proton transfer process. This secondary reaction is endoergic[10] and cannot proceed to the asymptotic separation of the products. Therefore, the $OH^-\cdot CH_3^\bullet$ intermediate isolated in these experiments is best regarded as an entrance-channel complex for the proton transfer reaction

$$OH^- + CH_3^\bullet \rightarrow H_2O + CH_2^{\bullet-}. \qquad (6)$$

The identification of the $OH^-\cdot HCH_2^\bullet$ complex as an intermediate in the proton transfer reaction provides a useful context in which to understand the origin of the strong red-shift associated with excitation of the shared proton. First, as is typical for the excitation of strongly H-bonded shared protons,[33−35] the bands associated with the motion are very broad, and both the dominant band at 2556 cm^{-1} and the companion feature about 200 cm^{-1} above it are much broader than the other bands appearing in the spectrum. To explore the nature of the potential surface that governs the O−H−C motion, we have performed preliminary calculations to extract the energy as a function of the hydrogen position. The resulting curve at the MP2/TZVPP level of theory is presented in Figure 6, indicating that the barrier for proton transfer is lower than the (harmonic) C−H stretching quantum (2620 cm^{-1}). This is similar to the scenario we encountered earlier in the $X^-\cdot H_2O$ (X = halide) complexes, where very basic anions lead to low barriers and even shelf potential functions resulting from intracluster proton transfer.[35,36] In those cases, the bands associated with the shared proton are often quite broad and are usually accompanied by combination bands associated with the ion−molecule stretch. In the $OH^-\cdot HCH_2^\bullet$ case, we expect such a combination band to occur with a spacing of about 200 cm^{-1} on the basis of the calculations (B3LYP/TZVP level), very close to the separation of the two broad bands assigned in Figure 2a to the excitation of the shared proton. Thus, we tentatively assign the weaker of the two broad features to the combination band arising from excitation of the $OH^-\cdot HCH_2^\bullet$ ion−radical stretching vibration along with the

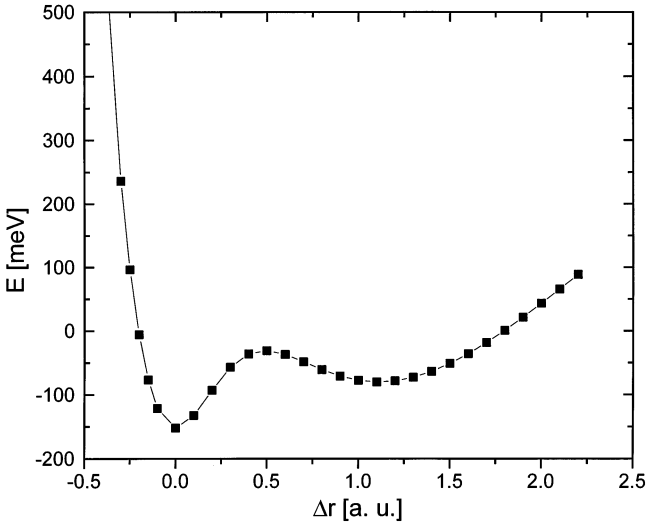

Figure 6. Calculated (MP2/TZVPP level of theory) potential energy curves for the proton transfer coordinate ($^-HO\cdots H^+\cdots CH_2^-$), obtained by scanning the C−H distance while allowing the other atoms to relax at each value.

1 ← 0 transition of the shared proton. Natural directions for future work are to explore whether the reaction can be photoinitiated starting from the bare (i.e., non-argon-solvated) complexes and to extend the method to larger alkanes. The latter is particularly attractive since temperature-controlled ion-flow tube experiments[5] have indicated that the proton transfer pathway becomes more important with the larger systems. Such studies are presently underway in our laboratory.

V. Summary

One of the two expected intermediates in the $O^{\bullet-} + CH_4 \rightarrow OH^- + CH_3^\bullet$ reaction has been isolated using argon cluster-mediated trapping of the collision complex. Vibrational predissociation spectroscopy indicates that this $[O\cdot CH_4]^{\bullet-}\cdot Ar_m$ species is an ion−radical adduct featuring a largely charge-localized hydroxide ion. Analysis of the rotational fine structure, however, establishes that the hydroxide ion is bound to one of the hydrogen atoms of the methyl radical in an $OH^-\cdot HCH_2^\bullet$ arrangement, rather than the $OH^-\cdot CH_3^\bullet$ (carbon-bound) exit-channel complex directly associated with the H-atom abstraction reaction. The rotational structure survives even upon addition of five argon atoms and only occurs upon excitation of the asymmetric $-CH_2$ stretching motion involving the nonbonded hydrogen atoms. Very red-shifted C−H stretching transitions are observed for excitation of the hydrogen atom bound to the ion, and the calculated potential surface for this motion indicates that the intracluster proton transfer reaction $OH^- + CH_3^\bullet \rightarrow H_2O + CH_2^-$ is accessible in the mid-IR region.

Acknowledgment. We thank the Experimental Physical Chemistry Division of the National Science Foundation (CHE-0111245) for their generous support of this work. J.M.W. thanks Prof. Dr. M. M. Kappes for generous support and the Emmy-Noether-Program of the Deutsche Forschungsgemeinschaft for financial help.

References and Notes

(1) Bohme, D. K.; Fehsenfeld, F. C. *Can. J. Chem.* **1969**, *47*, 2717.
(2) Comer, J.; Schulz, G. J. *Phys. Rev. A* **1974**, *10*, 2100.
(3) Viggiano, A. A.; Morris, R. A.; Miller, T. M.; Friedman, J. F.; M-Barreto, M.; Paulson, J. F.; Michels, H. H.; Hobbs, R. H.; Montgomery, J. A. *J. Chem. Phys.* **1997**, *106*, 8455.

(4) Viggiano, A. A.; Morris, R. A.; Paulson, J. F. *J. Chem. Phys.* **1988**, *89*, 4848.
(5) Arnold, S. T.; Morris, R. A.; Viggiano, A. A. *J. Phys. Chem. A* **1998**, *102*, 1345.
(6) Carpenter, M. A.; Farrar, J. M. *J. Chem. Phys.* **1997**, *106*, 5951.
(7) Lindinger, W.; Albritton, D. L.; Fehsenfeld, F. C.; Ferguson, E. E. *J. Chem. Phys.* **1975**, *63*, 3238.
(8) Goode, G. C.; Jennings, K. R. *Adv. Mass Spectrom.* **1974**, *6*, 797.
(9) Stockdale, J. A. D.; Compton, R. N.; Reinhardt, P. W. *Int. J. Mass Spectrom. Ion Phys.* **1970**, *4*, 401.
(10) Lee, J.; Grabowski, J. J. *Chem. Rev.* **1992**, *92*, 1611.
(11) Ervin, K. M.; Ho, J.; Lineberger, W. C. *J. Chem. Phys.* **1989**, *91*, 5974.
(12) Burnett, S. M.; Stevens, A. E.; Feigerle, C. S.; Lineberger, W. C. *Chem. Phys. Lett.* **1983**, *100*, 124.
(13) Olmstead, W. N.; Brauman, J. I. *J. Am. Chem. Soc.* **1977**, *99*, 4219.
(14) Cyr, D. M.; Scarton, M. G.; Johnson, M. A. *J. Chem. Phys.* **1993**, *99*, 4869.
(15) Dessent, C. E. H.; Bailey, C. G.; Johnson, M. A. *J. Chem. Phys.* **1996**, *105*, 10416.
(16) Kim, J.; Kelley, J. A.; Ayotte, P.; Nielsen, S. B.; Weddle, G. H.; Johnson, M. A. *J. Am. Soc. Mass Spectrom.* **1999**, *10*, 810.
(17) Robertson, W. H.; Kelley, J. A.; Johnson, M. A. *Rev. Sci. Instrum.* **2000**, *71*, 4431.
(18) Ayotte, P.; Weddle, G. H.; Kim, J.; Johnson, M. A. *Chem. Phys.* **1998**, *239*, 485.
(19) Wild, D. A.; Loh, Z. M.; Wolynec, P. P.; Weiser, P. S.; Bieske, E. J. *Chem. Phys. Lett.* **2000**, *332*, 531.
(20) Wild, D. A.; Loh, Z. M.; Bieske, E. J. *Int. J. Mass Spectrom.* **2002**, *220*, 273.
(21) Nielsen, S. B.; Ayotte, P.; Kelley, J. A.; Weddle, G. H.; Johnson, M. A. *J. Chem. Phys.* **1999**, *111*, 10464.
(22) Arnold, S. T.; Hendricks, J. H.; Bowen, K. H. *J. Chem. Phys.* **1995**, *102*, 39.
(23) Johnson, M. A.; Lineberger, W. C. In *Techniques for the Study of Ion−Molecule Reactions*; Farrar, J. M., Saunders, W. H. J., Eds.; Wiley: New York, 1988; Vol. 20; p 591.
(24) Frisch, M. J.; Trucks, G. W.; Schlegel, H. B.; Scuseria, G. E.; Robb, M. A.; Cheeseman, J. R.; Zakrzewski, V. G.; Montgomery, J. A., Jr.; Stratmann, R. E.; Burant, J. C.; Dapprich, S.; Millam, J. M.; Daniels, A. D.; Kudin, K. N.; Strain, M. C.; Farkas, O.; Tomasi, J.; Barone, V.; Cossi, M.; Cammi, R.; Mennucci, B.; Pomelli, C.; Adamo, C.; Clifford, S.; Ochterski, J.; Petersson, G. A.; Ayala, P. Y.; Cui, Q.; Morokuma, K.; Malick, D. K.; Rabuck, A. D.; Raghavachari, K.; Foresman, J. B.; Cioslowski, J.; Ortiz, J. V.; Stefanov, B. B.; Liu, G.; Liashenko, A.; Piskorz, P.; Komaromi, I.; Gomperts, R.; Martin, R. L.; Fox, D. J.; Keith, T.; Al-Laham, M. A.; Peng, C. Y.; Nanayakkara, A.; Gonzalez, C.; Challacombe, M.; Gill, P. M. W.; Johnson, B. G.; Chen, W.; Wong, M. W.; Andres, J. L.; Head-Gordon, M.; Replogle, E. S.; Pople, J. A. *Gaussian 98*; Gaussian, Inc.: Pittsburgh, PA, 1998.
(25) Ahlrichs, R.; Bär, M.; Häser, M.; Horn, H.; Kölmel, C. *Chem. Phys. Lett.* **1989**, *162*, 165.
(26) Schäfer, A.; Huber, C.; Ahlrichs, R. *J. Chem. Phys.* **1994**, *100*.
(27) Owrutsky, J. C.; Rosenbaum, N. H.; Tack, L. M.; Saykally, R. J. *J. Chem. Phys.* **1985**, *83*, 5338.
(28) *NIST Chemistry WebBook*; National Institute of Standards and Technology: Gaithersburg, MD, 2001.
(29) Ayotte, P.; Kim, J.; Kelley, J. A.; Nielsen, S. B.; Johnson, M. A. *J. Am. Chem. Soc.* **1999**, *121*, 6950.
(30) Bieske, E. J.; Dopfer, O. *Chem. Rev.* **2000**, *100*, 3963.
(31) Robertson, W. H.; Kelley, J. A.; Johnson, M. A. *J. Chem. Phys.* **2000**, *113*, 7879.
(32) Bailey, C. G.; Kim, J.; Dessent, C. E. H.; Johnson, M. A. *Chem. Phys. Lett.* **1997**, *269*, 122.
(33) Cabarcos, O. M.; Weinheimer, C. J.; Lisy, J. M.; Xantheas, S. S. *J. Chem. Phys.* **1999**, *110*, 5.
(34) Robertson, W. H.; Diken, E. G.; Price, E. A.; Shin, J.-W.; Johnson, M. A. *Science* **2003**, *299*, 1367.
(35) Robertson, W. H.; Johnson, M. A. *Annu. Rev. Phys. Chem.* **2003**, *54*, 173.
(36) Yates, B. F.; Schaefer, H. F., III; Lee, T. J.; Rice, J. E. *J. Am. Chem. Soc.* **1988**, *110*, 6327.